mm–Wave Collision Avoidance Sensors: Future Directions

D. C. Goodfellow, G. P. Harmer and D. Abbott

Centre for Biomedical Engineering (BME) and
Centre for High Performance Integrated Technologies and Systems (CHiPTec),
Department of Electrical and Electronic Engineering, The University of Adelaide,
SA 5005, Adelaide, Australia.

ABSTRACT

Passive millimeter–wave detection is advantageous for detection of objects obscured by rain, steam or other aerosols. This coupled together with collision avoidance techniques, based on biologically inspired insect vision models, promises compact low–cost solutions that do not require hardware–intensive image processing. This paper examines a number of possible future directions by identifying trade–offs between different integrated antenna strategies. Signal processing issues are also briefly discussed.

Keywords: Radiometry, Monolithic Fabrication, Motion Sensing, Insect Vision

1. INTRODUCTION

Since 1990 our group has been developing a movement detector on a single microchip, based on models[1–5] of how insects see. The rationale is that insects use very little visual computation (compared to humans) and yet can very efficiently avoid collisions. Using this approach enables a compact solution on a single microchip. Until recently our focus has been on applications in the automotive industry (eg. for driver blind-spot detection).[5]

However, over the past 2–3 years the interest of aerospace community, in our unique insect vision chip technology, has accelerated. Applications include:

- guidance for aircraft carrier landing systems
- guidance for miniature un–manned reconnaissance aircraft (useful for both military and environmental surveillance), known as micro–aerial vehicles (MAVs)[6]
- guidance for space vehicle docking systems
- collision avoidance for nanosatellite[7–10] clusters in space.

Nanosatellites are very small satellites in the 1–10 kg range. Future conventional satellites will be replaced by clusters* of these tiny satellites, in cases where redundancy and self–repair are important issues. For some applications the cluster can be designed to exhibit "collective behavior" rather like an insect colony, for the purposes of regrouping and/or adapting the effective communications aperture. Biologically inspired control systems for such clusters are also attracting interest.[11–13]

Recently we have been researching on performing insect vision in the mm-wave band as well as in the optical part of the spectrum – mm–waves penetrate the atmosphere more effectively than optical wavelengths and mm–wave detection is less prone to saturation effects in space. There is a window of opportunity to further research and investigate a fusion of these two approaches for leading-edge aerospace applications.

Other applications for the hardware include, collision avoidance and warning systems for commercial and public automobiles, landing or taxiing aircraft, close range all–weather object detection for ship docking and in–port navigation, industrial monitoring of manufacturing processes in obscured or dangerous environments, as well as some military applications, such as, missile seekers and synthetic vision for ground vehicles.

E-mail: dabbott@eleceng.adelaide.edu.au

*An example is the TechSat21 initiative: `http://www.vs.afrl.mil/VSD/TechSat21`

Part of the SPIE Conference on Sensing and Controls with Intelligent Transportation Systems
Boston, Massachusetts • November 1998
SPIE Vol. 3525 • 0277-786X/98/$10.00

2. MM–WAVE RADIOMETRY

Our proposed sensor utilizes radiometry which is the science of using passive detection techniques to detect background radiation.[14] Unlike a radar, which transmits a signal and then receives the backscattered radiation in order to measure various aspects of the scene of interest, a radiometer merely receives naturally occurring radiation. This natural radiation is simply part of the blackbody curve exhibited by all objects. The mm–wave band of interest can be seen in Fig. 1.

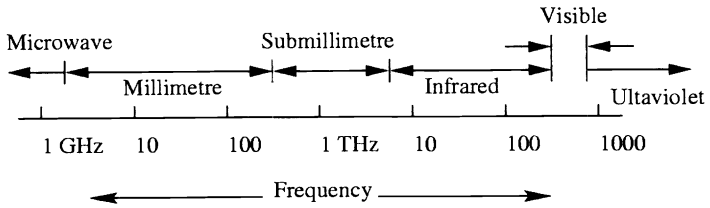

Figure 1. Electromagnetic spectrum.

By properly choosing the radiometer parameters, such as wavelength, polarization and viewing angle, it is possible to find relations between the magnitude of the energy received by the radiometer and specific parameters of the scene. The main parameter of interest is the *brightness temperature* T_B, which represents the intensity of the radiation emitted by the scene under observation. This brightness temperature may vary from zero Kelvin (for a non–emitting medium) to a maximum value equal to the physical temperature T_0 of the scene (for a perfect blackbody emitter). Another parameter of interest is the *emissivity*, $e = T_B / T_0$, which varies between zero and unity.

The applications for mm–wave radiometry include, (1) astronomical studies, (2) military applications and (3) environmental monitoring. In the cases of (1) and (3) the main interests lie in the measurement of background levels of emissivity. That is, measurements of naturally occurring sources of passive electromagnetic radiation. Whereas, in (2) the detection of man–made (*i.e.* metal) objects is of interest. Theoretically for a perfectly conducting material, such as metal, the emissivity is zero, so it is easy to differentiate from the Earth's background radiation, since the emissivity levels for land surfaces rarely fall below 0.3 and are often > 0.7. Physically, metal objects show non–zero radiometric temperatures, this is due to the reflection of downward–emitted sky radiation (electromagnetic energy from the Sun), not self–emission. Thus, the radiometric contrast between the *field of view (FOV)* and a metal target object contained in it is a function of the beam–fill factor (ratio of cross–sectional area of the metal target to the antenna *footprint* on the ground). The size of this footprint, essentially the spatial resolution of the antenna, is governed by the distance between the radiometer and the ground and by the beamwidth of the antenna. This spatial resolution is inherently limited at mm–wave frequencies, such that successful detection of a metal target can only be made within a few hundred meters. For obstacle avoidance in motor vehicles (the main application under consideration) this resolution is very good since the braking distance of an automobile is in the order of meters.

3. MM–WAVE SENSOR

By operating in the frequency range 30 – 100 GHz, advantage is taken of the ability to propagate over aerosol obscured paths. Advantage can also be taken of the ability to monolithically fabricate the mm–wave sensors and the reduction of the quality of the image processing needed for detection, which reduces the otherwise high cost of operating in this frequency band. That is, for the applications being discussed, it is possible to design the motion sensor without the need for many active components in the circuitry of the detector stage since insect vision motion detection requires less sensitivity than imaging, making the system simpler, less expensive, more compact and easier to fabricate.

Our strategy is to produce a mm–wave antenna array, operating at 37 GHz in the first instance, that can be monolithically fabricated, to include post–detection hardware. There exists two transmission 'windows' in the 30 – 100 GHz range, one at 37 GHz, the other at 94 GHz. That is, at these frequencies, the ability to passively sense mm–wave radiation over aerosol obscured paths, is realized. The design at the lower frequency of 37 GHz, will provide a low–cost testing platform, for a future scaled version of the design at the higher frequency of 94 GHz.

Preliminary test designs have been explored at 15 GHz.[15] These designs consisted of a number of substrate supported metal strip antenna elements, creating a linear array with a bandwidth of 10% and a FOV up to 90

degrees, allowable by the impedance and pattern characteristics of the designs. A prototype array, which operated at 15 GHz, consisting of a short focal length Rotman lens for beamforming, showed that care needed to be taken to avoid reflections that increase the sidelobe levels in the element patterns. The integrated antennas and low–loss beamforming network, was followed by low–noise mm–wave mixers, fabricated with suitable beam–lead *Schottky diodes*, to downconvert the signal.

From this design, it appears feasible, that with F/D = 1, a 37 GHz sensor can be designed consisting of a 15 element array with 15 beams, each having a beamwidth of 3°, overlapping at 3 dB points, and with sidelobes less than 10 dB using an alumina substrate. Thus, an array aperture of 50 mm at 37 GHz using hybrid fabrication techniques and of 22 mm at 94 GHz using wafer scale monolithic integration, should be achievable.

4. LENS DESIGN

A Rotman lens consists of a parallel–plate region with beam ports and array ports distributed along opposite contours, as shown conceptually in Fig. 2. By virtue of the design, a central beam port can provide equal path lengths to each array element. An off–set beam port (off–axis) will produce a path length and hence a phase gradient along the array giving a steered beam. With an equispaced array, a perfectly linear phase gradient along the array is realized for three beam directions, where beam ports are located at the focal points on the beam port contour.

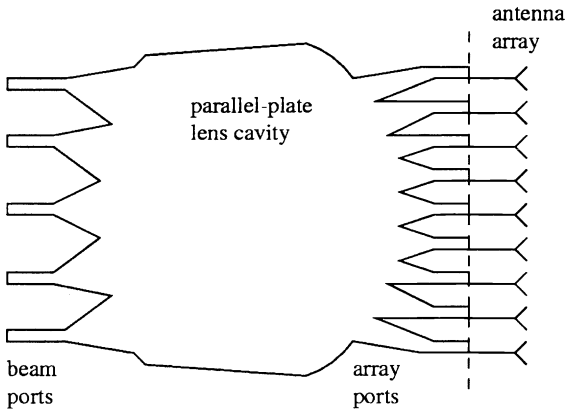

Figure 2. Schematic of 2D Rotman lens feeding a linear antenna array through a matching transistion line (shown dashed).

Several designs are possible for the system under consideration, where the decision on which to produce relies on factors such as the ease of fabrication, level of sensitivity needed to directly detect passive mm–radiation, cost and reliability. To realize a full MMIC design the system will use microstrip elements. That is, a folded dipole microstrip antenna array with microstrip lines feeding flared microstrip array ports of the lens (Fig. 2). The lens size must take into account the substrate used to construct the lens, where it must be reduced by the square root of the relative permittivity of the substrate ϵ_r. The plate separation of the lens is made less than half the wavelength inside the substrate ($\lambda_d/2$) therefore avoiding any twisting of the TEM mode which propagates through the parallel–plate region.

The design of a Rotman lens is governed by many different parameters.[16] Table 1 summarizes the values of these parameters for an alumina substrate ($\epsilon_r = 9.8$) filled lens operating at 37 GHz with a desired bandwidth of over 10%. Rotman and Turner[16] assumed that the internal lens angle θ was equal to the external beam angle ψ. A further degree of freedom in the lens design can be achieved if we assume that this is not the case producing a parameter called the beam to ray angle ratio, given by

$$\beta = \frac{\sin\psi}{\sin\theta}. \tag{1}$$

Table 1. 37 GHz lens design parameters.

Parameter	Value	Parameter	Value
frequency range	33–41 GHz	number of beams	15
angular coverage	90°	beamwidth	3°
adjacent beam cross–over level	3 dB	on–axis focal length, G	14.72 mm
		off–axis focal length, F	12.95 mm
element spacing	4.05 mm	center frequency	37 GHz
number of elements	15	beam/ray angle ratio, β	1.1
internal scan angle, α	30°	focal lengths ratio, g	1.137

We can then gain control over design parameters such as the array port spacing ($\beta \times$ array element spacing) near the center of the array port contour and the avoidance of waveguide cut–off at lower frequencies when $\beta > 1$. The size of the beam port apertures determines both the proportion of spill–over power and the number of beams produced.

The design of a particular strip transmission–line lens is first obtained in air, as per Rotman and Turner[16] for an air–filled parallel–plate lens, and the dielectric region is then scaled by the inverse square root of the substrate dielectric constant.[17] A very compact lens is possible if a substrate with high dielectric constant is used.

4.1. Metal design using MMIC technology

It is obvious that these methods do not absorb all of the spill–over energy and so a further method is to redesign the sidewall structure. In Rausch *et. al.*[18] the sidewalls were made triangular, that is the lens contours were linearly expanded until they met. This method 'traps' or confines the secondary beams in the triangular sidewall region until absorbed by the dummy ports, thus reducing the effect of these beams in the sidelobe response. A further extension of the sidewalls is to adopt a 'batman' configuration[15] of the lens, shown in Fig. 3. The wings on either side of the main lens structure serve to confine the spill–over energy more completely than the simple triangular configuration. Certain aspects of this design need to be carefully considered. The taper of the inlets into the side wings need to be constructed correctly so that energy from all possible incidence angles pass through the inlets.

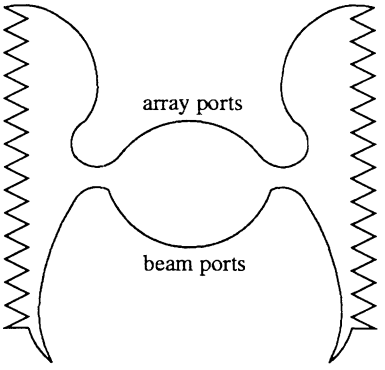

Figure 3. Rotman lens array in a 'batman' configuration.

The considerations discussed above will enable us to reduce the sidelobe levels of the system response satisfactorily. Yet, the multipath nature of the incumbent signals within the lens cavity is not the only mechanism for sidelobe production. The array and beam port design affect the close–in sidelobe levels. That is, the sidelobes adjacent to the main beam signature. As discussed above, the feed waveguides expand toward the lens cavity, which provides a better impedance match between the waveguides and the lens interior, similar to a horn transition. Within the tapers the energy received by adjacent ports through mutual coupling can be transferred in to higher order modes

if the point of maximum expansion at the waveguide lens cavity interface is not restricted in size to less than $\lambda_g/2$ (where λ_g is the wavelength inside the waveguide).

These higher modes will not propagate through the waveguides, which are designed to support only the TE_{01} mode, so they will be reflected back into the lens interior. This reflected energy will then interfere with the primary path energy, causing ripples along the ports (array ports for transmission, beam ports for reception). The slowly varying phase and amplitude ripples are the result of small differences in the signals of the primary and reflected paths and will create large close–in sidelobe patterns. A solution to negate this effect (*i.e.* if the taper needs to be wider than $\lambda_g/2$ for reasons of continuity of the lens contour as in Fig. 2) is to split each port into two ports and then combine the two ports at the output.[18] Many other design characteristics exist for the Rotman lens design, the implementations of which depend on the application.[19–23]

Initially the Rotman lens for this system is designed using Rotman and Turner's[16] design equations which are derived by viewing the geometry of the lens as in Fig. 4. Therefore, the amplitude and phase performance of the design can be calculated and it can then be determined whether this is of an acceptable level for this system. Fig. 5 shows the effects on the design at 37 GHz when different values for the normalized focal length ratio g are used. These values are 1.0, 1.1, 1.137 and 1.2 (where 1.137 is the optimum value determined by the relation $g = 1 + \frac{1}{2}\alpha^2$) and 30° off–axis focal point angle α. The values for X and Y coordinates and the transmission line lengths W for the optimum design are shown in Table 2 and the associated path length errors ΔL for different beam port placements at angles $\theta = 5°, 15°, 25°$ and 35° are shown in Fig. 6. As it can be seen the optimum value for g gives very small path length errors, not as small as those for $g = 1.1$ perhaps, but the response over all the elements is much 'flatter' meaning that the outer ports could be terminated, producing dummy ports, to eliminate these errors almost completely.

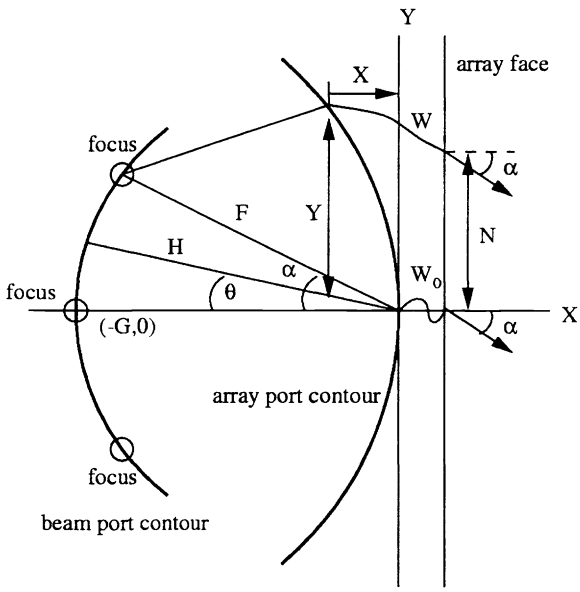

Figure 4. Rotman lens array and beam port contour geometries.

4.2. Plastic design

Another design possibility is use a completely plastic system, that is to build the sensor without the use of microstrip technology. To achieve this a dielectric rod antenna array feeds a dielectric Rotman lens with dielectric rod beam port feeds. These beam port rods taper into a waveguide regions that use small probes to extract the signal. A schematic diagram of a three dimensional view of such a system is shown in Fig. 7. The advantages of using such a system is its compact and durable nature.

Dielectric rod antennas can be successfully implemented in integrated circuit design[24] and offer small size, economy and high gain characteristics. Many forms of dielectric rods exist with the most common being the leaky–wave

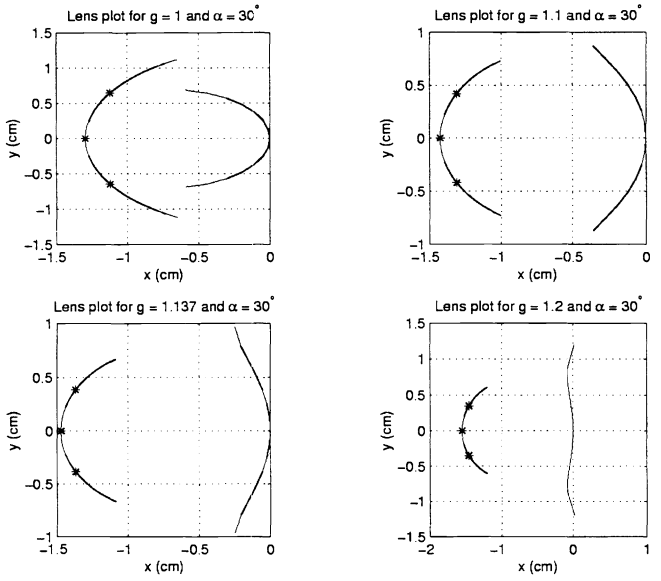

Figure 5. Rotman lens beam port (right) and array port (left) curve designs at 37 GHz for values of $g = 1.0, 1.1, 1.137$ (optimum) and 1.2, with $\alpha = 30°$ and radius and center positions of the beam port contour circles 12.95 and 0.0, 8.43 and -5.81, 7.73 and -6.99 and 7.01 and -8.53 mm respectively.

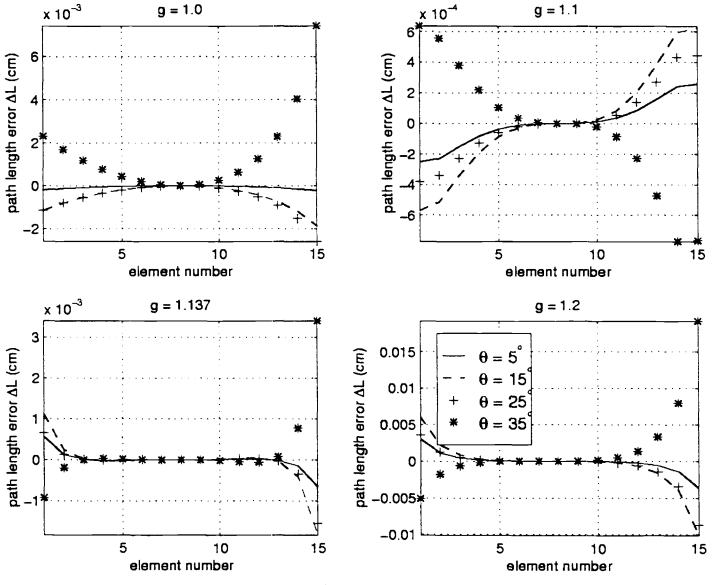

Figure 6. Path length errors for different angular positions of beam ports for the Rotman lens designs in Fig. 5.

Table 2. 37 GHz Rotman lens design parameters for $g = G/F = 1.137$ and $\alpha = 30°$. These are the normalized array element position $\eta = N/F$, array port transmission line length $W - W_0 = Fw$ (where W_0 is the transmission line length between the on–axis array port and w is the normalized difference between the off–axis and on–axis transmission line lengths) and array element and the X and Y coordinates of the array port on the array port contour.

η (cm)	W (cm)	X (cm)	Y (cm)
0.0000	0.0000	0.0000	0.0000
0.1295	0.0005	-0.0063	0.1294
0.2590	0.0020	-0.0249	0.2586
0.3885	0.0035	-0.0556	0.3874
0.5180	0.0035	-0.0974	0.5166
0.6475	-0.0018	-0.1484	0.6484
0.7770	-0.0222	-0.2038	0.7904
0.9065	-0.0898	-0.2473	0.9694

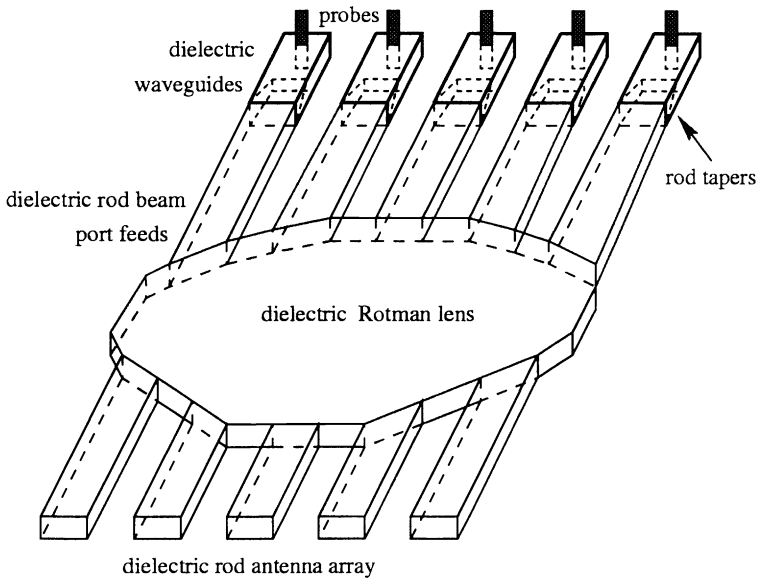

Figure 7. Schematic of three dimensional fully plastic Rotman lens array design.

antennas.[25,26] The characteristics of the signal propagation in these dielectric rod waveguides is well understood and so the design of such is reasonably unlimited. The schematic in Fig. 7 shows the dielectric rod apertures angled at the array port contour, this angle is used to allow a linear array aperture without bending the rod antennas which could cause phase errors and is more difficult to fabricate. The characteristics of the TEM mode signal leaving the open–end of this angle rod is well understood and has been determined experimentally for microstrip technology.[27] With this process in mind the array ports are to be placed so as to give the desired beam angles in the lens medium.

The beam port dielectric rod apertures are similarly angled at the lens beam port contour, to allow a parallel back–end. These beam port rods are tapered in one dimension into a rectangular waveguide region so that none of the signal is lost due to the transition from the dielectric rod region to the rectangular waveguide region. Different taper designs are possible and have their own merits, the choice of which type depends on the gain and sidelobe levels needed for the application.

5. SIGNAL PROCESSING ISSUES

As shown in Fig. 8, the beam output is to be firstly amplified and then integrated, for a certain dwell time. The dwell time can be varied to enhance the signal-to-noise ratio. The signal is then sampled and undergoes a temporal differentiation in the digital domain. Although differentiation in the analog domain is possible, it is problematic for future IC realization of the circuitry. This arises from the large time constants needed (in the order of ms) resulting in large passive component values.

After differentiation, the signal is then thresholded, enabling simple 2 by 2 motion templates to be formed between adjacent channels from two samples in time. Higher order templates are possible when more than 15 channels are realized in the future. Within each 2 by 2 template an up-arrow indicates increasing detected signal, a down-arrow indicates decreasing signal and a dash indicates no-change. From these templates, the bearing and time-to-impact of a detected object can be inferred.[1–5]

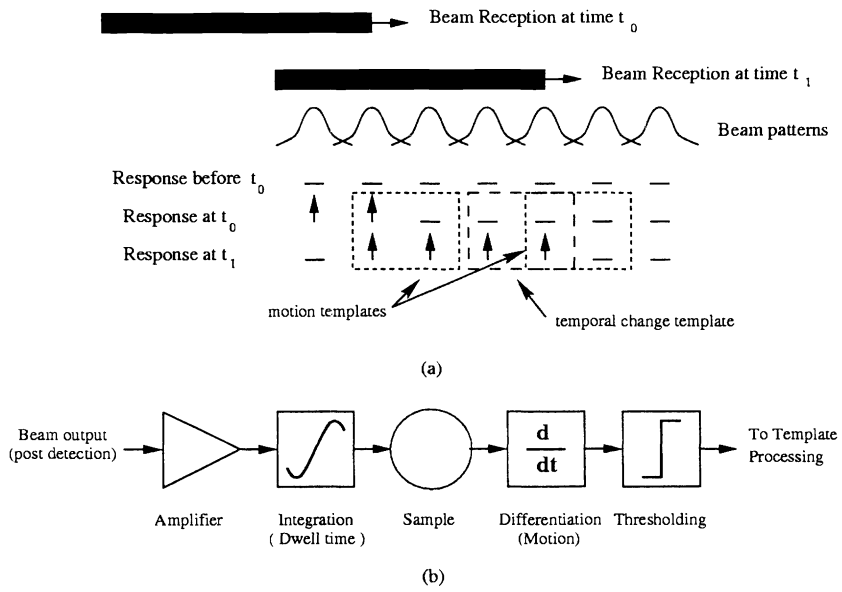

Figure 8. Insect vision processing. (a) Formation of motion templates (b) Front-end processing.

The thresholding operation, inherent in insect vision, can be exploited to enhance the signal in the presence of noise. This cooperative effect of noise in non-linear systems is term stochastic resonance.

5.1. Stochastic Resonance

Noise in dynamical systems is usually considered a nuisance. However, in certain nonlinear systems, including electronic circuits and biological sensory systems, the presence of noise can enhance the detection of weak signals.

The phenomenon is termed stochastic resonance. When noise is added to a system, the output usually deteriorates in quality. However, in some systems, adding the right amount of noise can enhance the system output or response. For these systems, it can be shown that there exists a non-zero value of noise that gives an optimal value for the signal-to-noise ratio (SNR) of the system.

What is stochastic resonance (SR)? Stochastic resonance can be characterized by the response of a system to noise, the signal-to-noise ratio. The SNR rises sharply to a maximum value then gradually decreases for higher noise intensities, where SR occurs, as noise is added to a system. More formally, it is a noise-mediated cooperative phenomenon, manifest in non-linear systems, wherein the response to a deterministic signal can be enhanced in the presence of an optimal amount of noise.

It is seen from this description of SR that it is not strictly a resonance as the increased response is *not* due to a natural frequency of the system. The alternative use of the word *resonance* is derived from the SNR having a peak due to some other parameter – in this case, input noise amplitude.

The essential ingredient for SR is a nonlinear dynamical system, which typically has a periodic signal and noise at the input, and an output that is a function of the inputs as well as the internal dynamics of the system. The nonlinear component of the dynamical system is sometimes provided by a threshold which must be crossed for the output to be changed or detected.

A two–state system in common use for SR is the threshold system. This is a simple system that produces an output voltage when ever the input exceeds the threshold value. In biological systems it is referred to as a fire-and-reset model and works by sending a pulse of fixed width when ever the signal in question exceeds a certain threshold.

A closer look reveals that this is a variation of the Schmitt trigger. A threshold system can be implemented with the Schmitt trigger by adding some bias and keeping the thresholds very close together. Although there are two types of bistable systems, continuous and discrete, it is not obvious how to compare the results between them .[28]

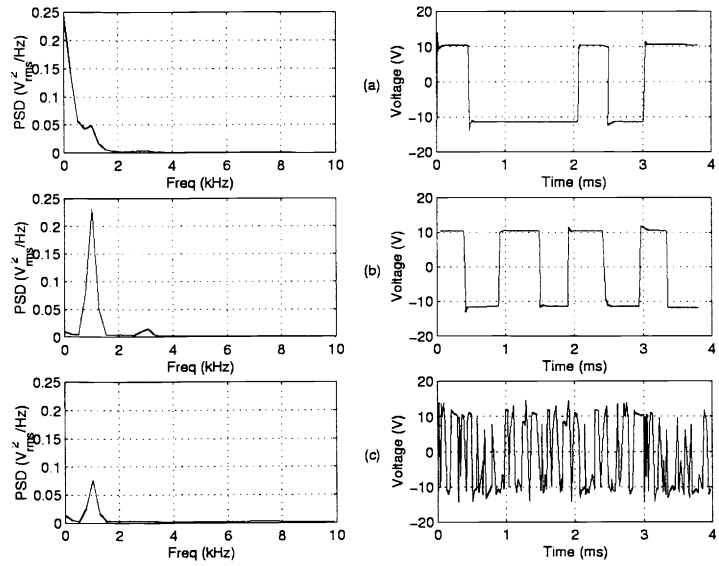

Figure 9. Comparing the frequency and time domain as the noise is increased. In (a) only low noise has been added, causing intermittent transitions. Adding optimal amount of noise in (b) causes regular transitions, and adding high noise in (c) causes the transitions to be dominated by the noise.

The MATLAB simulation in Fig. 9 illustrates the phenomenon of stochastic resonance in the frequency and time domain. The first time-domain graph shows a near-threshold signal 'misfiring,' but when noise is added, the restored signal is shown in the second graph. The third graph shows that too much noise swamps the signal. Hence, an

optimum quantity of noise is required to maximize the information content. This is more dramatically illustrated in the frequency-domain – where the second graph, as expected, shows the strongest peak at the fundamental frequency.

In most physical systems the signal and noise are fixed with a threshold at the receiver being variable. Even though noise could be added at the receiver in order to get an increase in SNR, it is not going to be as good as using the minimal amount of noise possible and changing the threshold. Rather than thinking in terms of finding the optimal noise value for a given threshold, it may be more useful to think of SR in terms of finding the optimal threshold for given noise. Thus, in order for SR to be useful for a physical application, we ideally need a system with a threshold, but where the value of the threshold is not critical to the output.

This naturally lends itself to a binary threshold system with the output being in either of one of two states. It has been demonstrated that the information capacity in an asymmetric binary channel reaches at a maximum with the addition of noise[29] the effects of varying the thresholds are also shown.

Another area of interest of SR is in signal processing where weak signals are embedded in noise. SR can be used to enhance the signal-to-noise ratio of the output making it useful in a receiver. These signals need not be periodic as SR has been displayed to be present in non-periodic signals.[30]

For insect vision, motion is determined by detecting edges in the image plane and comparing them over time. In this case the signals from the insect vision sensor can be noisy. Edges that are determined by comparing different pixels to a threshold could use SR to enhance their detection. Since the noise varies spatially as well as temporally, a large improvement in the image quality is expected.[31] Such schemes may prove critical in the initiative to perform insect vision processing in the millimeter–wave region.[15]

6. CONCLUSION

An extension of our work on optical insect vision detectors, into the mm-wave domain, is promising for a number of applications – particularly in aerospace. Both metal-on-substrate and dielectric antenna schemes are discussed. If successful, dielectric antennas could prove to be a low-cost approach – there would also be clear benefits for efficient mass production. The insect vision model requires the signals to be thresholded – and we point out that this non-linearity can be exploited to improve the signal response, via stochastic resonance.

ACKNOWLEDGMENTS

This work has been kindly funded by the Australian Research Council (ARC). We warmly thank Dr. A.J. Parfitt, now at CSIRO, Sydney, for his generous guidance and much of the inspiration on the integrated antenna aspects.

REFERENCES

1. D. Abbott, A. Bouzerdoum, and K. Eshraghian, "Two-dimensional smart arrays for collision avoidance," *Proc. SPIE* **3207**, pp. 36–39, 1997.
2. D. Abbott, A. Bouzerdoum, and K. Eshraghian, "Future directions for motion detection based on the parallel computational intelligence of insects," *Proceedings. 23rd Euromicro Conference New Frontiers of Information Technology - Short Contributions* , pp. 244–249, 1997.
3. D. Abbott, A. Moini, A. Yakovleff, X. T. Nguyen, R. Beare, W. Kim, A. Bouzerdoum, R. E. Bogner, and K. Eshraghian, "Status of recent developments in collision avoidance using motion detectors based on insect vision," *Proc. SPIE* **2902**, pp. 242–247, 1997.
4. A. Moini, X. T. Nguyen, A. Blanksby, R. Beare, D. Abbott, and R. E. Bogner, "An insect vision-based motion detection chip," *IEEE Journal of Solid-State Circuits* **32**(2), pp. 279–284, 1997.
5. D. Abbott, A. Moini, X. T. Nguyen, A. Blanksby, R. Beare, A. Beaumont-Smith, G. Kim, A. Bouzerdoum, R. E. Bogner, and K. Eshraghian, "Biologically inspired obstacle avoidance-a technology independent paradigm," *Proc. SPIE* **2591**, pp. 2–12, 1995.
6. W. R. Davis, B. B. Kosicki, D. M. Boroson, and D. F. Kostishack, "Micro air vehicles for optical surveillance," *Lincoln Laboratory Journal* **9**(2), pp. 197–214, 1996.
7. J. R. Stuart and J. G. Stuart, "Revolutionary next generation satellite communications architectures and systems," *1997 IEEE Aerospace Conference. Proceedings* **3**, pp. 535–545, 1997.
8. A. Hansson, "From microsystems to nanosystems," *J. British Interplanetary Society* **51**, pp. 123–126, 1998.

9. J. R. Stuart, R. R. Coffey, and J. G. Stuart, "Economics of the new smaller and shorter lifetime geostationary communications satellites," *Pacific Telecommunications Council Fifteenth Annual Conference* **2**, pp. 531–536, 1993.
10. S. Meuncheburg, M. Krischke, and N. Lemke, "Nanosatellites and micro systems technology – capabilities, limitations and applications," *Acta Astronautica Proc. 1996 IAA Internat. Symposium on Small Satellites for Earth Observation* **39**, pp. 799–808, Nov. 1996.
11. J. R. Frigo and M. W. Tilden, "Analog neural network control method proposed for use in a backup satellite control mode," *Proc. SPIE* **3210**, pp. 84–94, 1998.
12. J. R. Frigo and M. W. Tilden, "SATBOT I: prototype of a biomorphic autonomous spacecraft," *Proc. SPIE* **2591**, pp. 66–75, 1995.
13. B. Hasslacher and M. W. Tilden, "Living machines," *Robotics and Autonomous Systems* **15**(1-2), pp. 143–169, 1995.
14. F. T. Ulaby, R. K. Moore, and A. K. Fung, *Microwave Remote Sensing: active and passive, Vol. 1: Microwave remote sensing fundamentals and radiometry*, Addison–Wesley Publishing Company, USA, 1981.
15. D. Abbott and A. Parfitt, "Extension of the insect vision paradigm to millimeter waves," *Proc. SPIE* **3207**, pp. 103–106, (Pittsburgh, PA), Oct. 1997.
16. W. Rotman and R. F. Turner, "Wide-angle microwave lens for line source applications," *IEEE Trans. Antennas Propagat.* **AP-11**, pp. 623–632, Nov. 1963.
17. D. R. Gagnon, "Procedure for correct refocusing of the rotman lens according to snell's law," *IEEE Trans. Antennas Propagat.* **AP-37**, pp. 390–392, Mar. 1989.
18. E. O. Rausch, A. F. Peterson, and W. Wiebach, "Electronically scanned millimeter wave antenna using a rotman lens," *Proc. of Radar Systems (RADAR '97)* , (Edinburgh, UK), Oct. 1997.
19. S. F. Piek and J. Heinstadt, "Multiple beam microstrip array fed by rotman lens," *Ninth Int. Conf. Ant. Prop.* **1**, pp. 348–351, (Eindenhoven, Netherlands), Apr. 1995.
20. P. G. Rogers, "Design of compact low-loss rotman lenses," *IEE Proc. H* **134**, pp. 449–455, Oct. 1987.
21. T. Katagi, S. Mano, and S.-I. Sato, "An improved design method of rotman lens antennas," *IEEE Trans. Antennas Propagat.* **AP-32**, pp. 524–527, May 1984.
22. M. S. Smith, "Multiple beam crossovers for a lens-fed antenna array," *J. IERE* **55**, pp. 33–36, Jan. 1985.
23. H. L. Southall and D. T. McGrath, "An experimental completely overlapped subarray antenna," *IEEE Trans. Antennas Propagat* **AP-34**, pp. 465–474, Apr. 1986.
24. Y. Shiau, "Dielectric rod antennas for millimeter–wave integrated circuits," *IEEE Trans. Micro. Theory and Techniques* **MTT-24**, pp. 869–872, Nov. 1976.
25. R. Mittra and R. Kastner, "A spectral domain approach for computing th eradiation characteristics of a leaky-wave antenna for millimeter waves," *IEEE Trans. Antennas Propagat* **AP-29**, pp. 652–654, July 1981.
26. S. Kobayashi, R. M. R. Lampe, and S. Ray, "Dielectric rod leaky-wave antenna for millimeter–wave applications," *IEEE Trans. Antennas Propagat* **AP-29**, pp. 822–824, Sept. 1981.
27. L. Musa and M. S. Smith, "microstrip port design and sidewall absorption for printed rotman lenses," *IEEE Proc. H.* **136**, pp. 53–58, Feb. 1989.
28. B. McNamara and K. Wiesenfeld, "Theory of stochastic resonance," *Physical Review A* **39**, pp. 4854–4869, May 1989.
29. F. Chapeau-Blondeau, "Noise-enhanced capcity via stochastic resonance in an asymmetric binary channel," *Physical Review E* **55**, pp. 2016–2019, Feb. 1997.
30. L. Gammaitoni, P. Hänggi, P. Jung, and F. Marchesoni, "Stochastic resonance," *Reviews of Modern Physics* **70**, pp. 223–287, Jan. 1998.
31. E. Simonotto, M. Riani, S. Charles, M. Roberts, J. Twitty, and F. Moss, "Visual perception of stochastic resonance," *Physical Review Letters* **78**, pp. 1186–1189, Mar. 1997.